Spectrochimica Acta Part B 87 (2013) 65–73

Contents lists available at ScienceDirect

Spectrochimica Acta Part B

journal homepage: www.elsevier.com/locate/sab

Role of laser pre-pulse wavelength and inter-pulse delay on signal enhancement in collinear double-pulse laser-induced breakdown spectroscopy

P.K. Diwakar *, S.S. Harilal, J.R. Freeman, A. Hassanein

Center for Materials Under Extreme Environment, School of Nuclear Engineering Purdue University, West Lafayette, IN 47907, USA

ARTICLE INFO

Article history:
Received 4 December 2012
Accepted 12 May 2013
Available online 21 May 2013

Keywords:
LIBS
Double pulse LIBS
Plasma diagnostics
LPP

ABSTRACT

Dual-pulse (DP) laser-induced breakdown spectroscopy (LIBS) provides significant improvement in signal intensity as compared to conventional single-pulse LIBS. We investigated collinear DPLIBS experimental performance using various laser wavelength combinations employing 1064 nm, 532 nm, and 266 nm Nd:YAG lasers. In particular, the role of the pre-pulse laser wavelength, inter-pulse delay times, and energies of the reheating pulses on LIBS sensitivity improvements is studied. Wavelengths of 1064 nm, 532 nm, and 266 nm pulses were used for generating pre-pulse plasma while 1064 nm pulse was used for reheating the pre-formed plasma generated by the pre-pulse. Significant emission intensity enhancement is noticed for all reheated plasma regardless of the pre-pulse excitation beam wavelength compared to single pulse LIBS. A dual peak in signal enhancement was observed for different inter-pulse delays, especially for 1064:1064 nm combinations, which is explained based on temperature measurement and shockwave expansion phenomenon. Our results also show that 266 nm:1064 nm combination provided maximum absolute signal intensity as compared to 1064 nm:1064 nm or 532 nm:1064 nm.

1. Introduction

Laser-induced breakdown spectroscopy (LIBS) technique is useful for a variety of applications including elemental analysis, detecting airborne biological agents, quantitative analysis of aerosols etc. [1–3]. Although LIBS is suited for various applications, this technique possesses lower sensitivity and precision than the other forms of elemental analysis. Improvements in the sensitivity of LIBS can be achieved by enhancing the signal strength or reducing the background noise. Recent advancements with femtosecond (fs) laser based LIBS and polarization resolved LIBS showed sharp reduction in background continuum noise, but the technology of a handheld fs laser system is still far away [2,4,5]. Among the various methods proposed for improving the detection sensitivity of LIBS, double-pulse (DP) excitation is more promising [6–11]. The term "double-pulse" can be defined as follows; two laser pulses used for LIBS excitation, which are separated in time by a period of few nanoseconds to several microseconds. Quite recently, several research groups explored applications for DP because of advances in laser technology and better analytical detection systems [3,6,9,11–15]. Double pulses have been found to increase LIBS sensitivity for the analysis of liquids [16], solids immersed in liquid [17], and solids [18,19]. Apart from analytical applications, DP technique has been used in laser-produced plasma (LPP) for x-ray [20,21] and EUV emission enhancement [22,23]. The DP emission enhancement in the x-ray and soft x-ray regions of the electromagnetic spectrum has potential applications in the fields of microscopy, lithography and x-ray laser.

Compared to single-pulse LIBS, DPLIBS contains several additional experimental parameters for controlling the resulting plasma evolution and emission and one of them is the angle of pre-pulse and reheating laser beams. Several methods have been utilized for performing DP experiments in LIBS and some of these schemes are shown in Fig. 1. In collinear double pulse experiments, both beams approach orthogonal to the target. This is the simplest approach from a practical point of view [16,24]. In the orthogonal reheating arrangements, the first pulse is used to ablate the sample and create a plume, and the second pulse is utilized for reheating the plume [25]. In the orthogonal pre-ablation LIBS set up, the first beam is irradiated parallel to the sample surface, generating a spark in the ambient atmosphere, and the second pulse is directed orthogonal to the target surface [26]. Kuwako et al. [27] used a DP crossed beam approach for improving the detection sensitivity of LIBS and a similar scheme is also used in Townsend effect plasma spectroscopy [28,29].

Even though DPLIBS experiments provided higher sensitivity, there exists some controversy in explaining the exact mechanism causing the improved sensitivity. Noll et al. [10] claimed that intense and long lasting emissions from collinear LIBS analysis are not due to reheating of the plasma, but are caused by a higher mass ablation rate, and hence large plasma volume. On the contrary, Uebbing et al.

* Corresponding author.
E-mail addresses: pdiwakar@purdue.edu, pdiwakar@gmail.com (P.K. Diwakar).

0584-8547/$ – see front matter © 2013 Elsevier B.V. All rights reserved.
http://dx.doi.org/10.1016/j.sab.2013.05.015

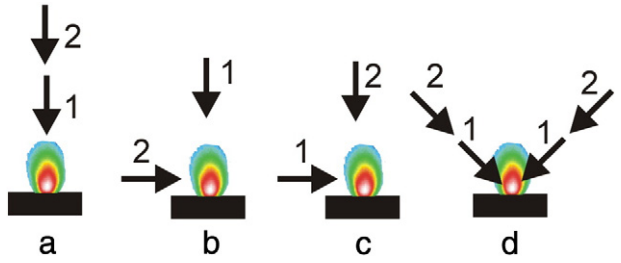

Fig. 1. Various DP geometries used for LIBS. The arrows show the sequence and direction of the laser pulses. (a — collinear LIBS; b — orthogonal reheating; c — orthogonal pre-ablation LIBS; and d — dual pulse crossed beam LIBS).

[30] observed a considerable enhancement in the signal intensity with orthogonal reheating scheme. Stratis et al. [31] performed DP experiments in the reverse temporal order with respect to the work of Uebbing [30] and observed large increases in the amount of material ablated during the pre-ablation spark experiments. However, the mechanism that leads to the enhanced ablation was unknown. Hahn's group [32] also explored the pre-spark orthogonal DP scheme, and their transmission studies showed that there was no change in the laser–target and laser–plasma coupling comparing single-pulse and dual-pulse configurations. Cristoforetti et al. [24] noticed the DPLIBS signal enhancement depended strongly on the ambient pressure and interpreted this to the balance between laser shielding and plume confinement with different ambient pressure levels. Sabsabi and co-workers [18,19] reported that higher sensitivities can be achieved by using a sequence of UV and NIR wavelengths compared to same wavelength DP experiments. Recent DPLIBS employing YAG and TEA CO_2 lasers showed a signal enhancement of more than 300 times, a technique referred to as Townsend effect plasma spectroscopy (TEPS) [28,33]. The sharp increase in the TEPS is attributed to prolonged heating of the plasma by the long temporal tail of the TEA CO_2 laser. Russo and co-workers [34] systematically investigated LIBS plasma properties versus delay time between two laser pulses and found that the plasma properties as well as the crater dimensions increased abruptly when the delay between the pulse was between 100 and 200 ns, and suggested that liquid layer instability and phase explosion are two possible mechanisms behind this.

Most of the articles in DPLIBS highlight significant improvement in LIBS sensitivity, even in the simplest configuration involving two identical lasers [6,28,35]. For optimizing LIBS performance, researchers have varied time delay and energy in the pre- and main pulses, used different experimental geometries, and changed the pressure of the ambient gas. It is interesting to note that with collinear DP geometry, the reported signal improvement varied from a factor of 2 to 100 [18,36–38]. However, the reasons for the increased sensitivity have not been yet univocally ascertained and little effort has been paid to understand the physics behind this emission enhancement. A thorough understanding of the plasma dynamics is a must for improving the sensitivity of LIBS. In this study, plasma spectroscopy and optical diagnostic tools have been used for characterizing the signal enhancement in collinear double pulse LIBS (DPLIBS). Specifically the role of pre-pulse laser wavelength, energy, and inter-pulse delay has been studied using brass as a sample. The observations in combination with earlier studies by other groups provide better understanding of the mechanisms involved in signal enhancement for collinear DPLIBS.

2. Experimental set up

Two Nd:YAG lasers operating at 10 Hz were used for all the experiments. Three wavelengths were used for first laser pulse (1064 nm, 532 nm, 266 nm, full width half maximum, FWHM 6 ns), hereby referred to as *laser 1* or *pre-pulse laser* while the wavelength of the second laser pulse, hereby referred to as *laser 2*, was kept constant at 1064 nm (6 ns FWHM). The energy of both the laser beams was adjusted using a combination of half wave plate and polarizing cube which allowed attenuation of laser pulse energy without causing laser pulse duration or spatial profile modifications. The laser beams were carefully aligned and then focused to a tight spot on the target in collinear arrangement. Spot size of *laser 1* was ~100 μm while that of *laser 2* was ~1 mm. This arrangement was designed so as to allow sufficient spatial reheating of the plasma formed by first laser pulse. Brass target mounted on XYZ stage allowed movement of the target to provide fresh ablation sites for each set of experiments thereby eliminating any drilling or crater effect from earlier experiments. A schematic of the experimental set up is shown in Fig. 2. Timing between the two laser pulses was controlled using digital delay generators. The experiments were performed in single shot mode but the flash lamps of both the lasers were continuously run at 10 Hz to avoid beam expansion caused by thermal lensing effects. Adjusting the delay generator allowed firing of laser pulses simultaneously or at different inter-pulse delays ranging from few hundred nanoseconds to microseconds. The delay between the laser pulses was monitored using a fast rise detector and oscilloscope. The delay between laser flash lamp and Q-switch of both the lasers was kept constant through the experiment to maintain stable and constant laser beam characteristics. The distance between the target and collecting lens was fixed for all the wavelengths. It should however be noted that variable focusing and collection distance can result in optimum signal measurement. Plasma emission was collected using a 40-cm lens, which focused the light on to the slit of high-resolution 0.5 m Czerny–Turner spectrograph (0.025 nm resolution). The emission was detected in the range of 200–900 nm using different gratings. Specifically, 1800 grooves/mm was used for electron density measurements, while 150 grooves/mm was used for temperature measurement using Boltzmann plots and intensity measurements. Cu I lines at 427.51, 465.11, 510.55, 515.32, and 521.82 nm were used for plasma excitation temperature estimation. An intensified charged couple device (ICCD) detector was used for collecting the dispersed light signal. The ICCD was synchronized to the Q-switch delay of *laser 2*, so that emission observed was always after both the lasers were fired. For data acquisition, a fixed gate delay of 1.4 μs was used while gate width of 20% of gate delay was used which in this case was 280 ns. Single pulse LIBS signal using 50 mJ energy for different wavelengths was used for identifying optimum gate pulse delay which was found to be ~1.4 μs. For double pulse experiments, same gate pulse delay was used for signal intensity comparison. A photomultiplier tube (PMT, 1 ns rise time) was used for measurement of lifetime or persistence of copper and zinc species present in the plasma. Focused shadowgraphy employing 532 nm probe beam was used for obtaining the shadowgrams and ICCD was used for recording plume images of the pre-plasma [39].

3. Results and discussions

3.1. Signal enhancement

Fig. 3 shows significant enhancement in LIBS signal for YAG–YAG combination in collinear arrangement for fundamental wavelength combination. Prepulse laser energy (E_{laser1}) is fixed at 25 mJ for all the wavelengths, while the second laser pulse energy (1064 nm) was varied from 50 to 75 mJ (E_{laser2}). For all the comparisons showed here, the total energy input is kept constant for both single pulse and double pulse LIBS ($E_{single\ pulse} = E_{double\ pulse} = E_{laser1} + E_{laser2}$). Brass was chosen as sample for this study. Spot size of ~100 μm was used for the first laser pulse while spot size of ~1 mm was used for reheating laser pulse. By observing the raw data, it can be clearly seen that there is enhancement in signal intensity (~15×) for collinear DPLIBS. Enhancement in signal intensity of neutral species is

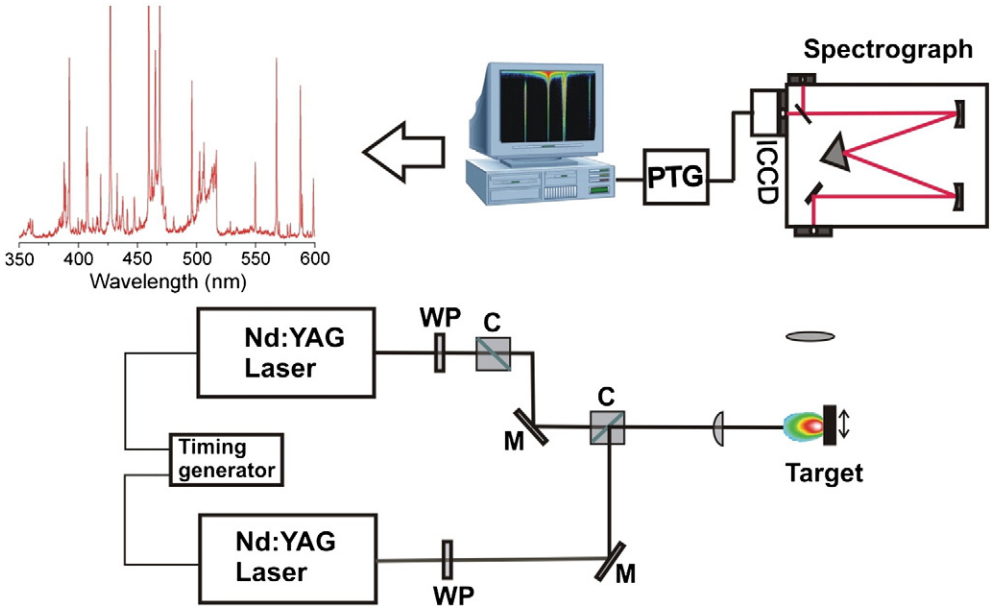

Fig. 2. Schematic of the experimental set up (WP, wave plate; C, polarizing cube; M, laser mirror; PTG, programmable timing generator; ICCD, intensified CCD).

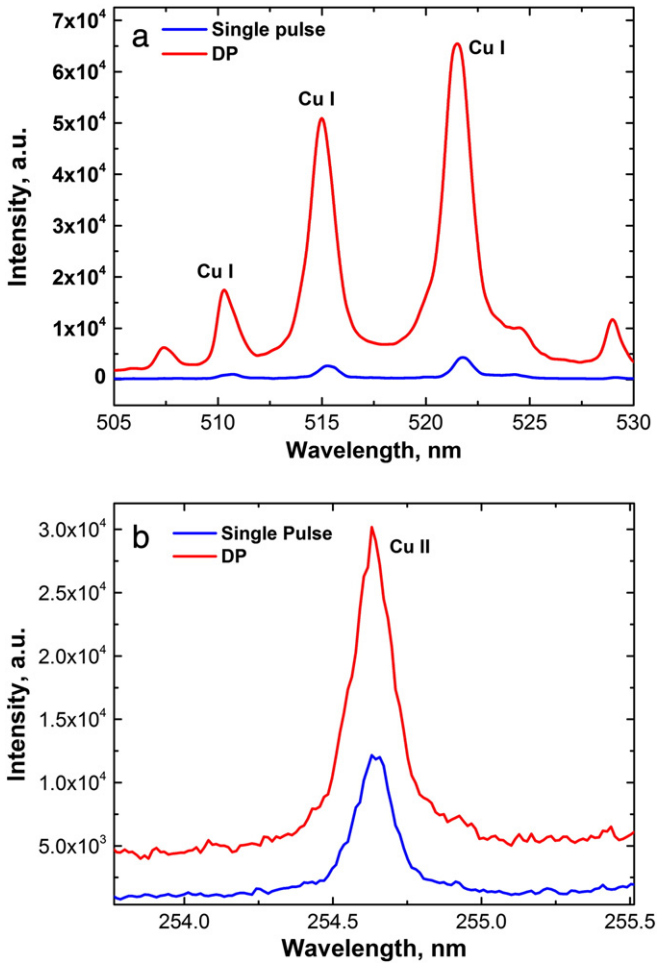

Fig. 3. Comparison of DPLIBS (YAG–YAG collinear scheme; 1064 nm–1064 nm) signal intensity with single pulse LIBS for (a) neutral Cu species and (b) Cu ionic species. Prepulse laser energy (E_{laser1}) was 25 mJ while the second laser pulse energy (E_{laser2}) was 75 mJ. For comparison, single pulse energy of 100 mJ ($E_{laser1} + E_{laser2}$) was used. Cu I lines at 510.5 nm, 515.3 nm and 521.8 nm from the brass sample are shown in (a) while Cu II emission at 254.6 nm is shown in (b). A gate delay of 1.4 μs after the second laser pulse and inter-pulse delay of 1200 ns was used for data acquisition.

considerable, although it has to be noted that background emission is also higher in the DP scheme which can be due to increased mass ablation, efficient laser–plasma coupling and reheating. Enhancement in signal intensity of ionic species is also observed although the enhancement is not as dramatic as for the neutral species. It must be noted that fixed gate delay of 1.4 μs (after the second laser pulse) was used for both neutral and ionic species. Signal enhancement is shown to be dependent on gate delay and it is possible that optimum gate delay will be different for ionic and neutral species. It should also be noted that optimum gate pulse delay will be different for different wavelengths and laser pulse energies, however for limiting the experimental parameters, a fixed gate delay was used. By optimizing gate pulse delay for DPLIBS, it may be possible to have even further signal enhancement.

3.2. Role of inter-pulse delay

Inter-pulse delay plays an important role in signal enhancement in any DPLIBS scheme as it dictates the laser–target and laser–plasma interactions thereby influencing the ablation efficiency and plasma re-heating processes. Fig. 4a shows the role of inter-pulse delay in signal enhancement for the collinear pulsed arrangement used in the current study. Signal intensity from DPLIBS was normalized to single pulse LIBS. In literature, signal enhancement has been reported in different ways [32] (peak sum, absolute peak sum, peak height with base subtracted). For comparison, we have reported the signal enhancement in all the three schemes. Overall the signal trend is same for all the three cases. It can be seen that there is signal enhancement even for zero ns pulse delay. First peak is observed at around 250 ns and then there is a decrease in signal enhancement around 900 ns followed by second maxima at ~1400 ns. After 1400 ns a constant enhancement is observed. Similar dip in signal enhancement has been observed by Cristoforetti et al. [40] in pre-orthogonal double pulse configuration.

Various mechanisms have been proposed for signal enhancement in collinear DPLIBS arrangement that includes either increase in mass ablation or reheating of the plasma plume or a combination of both the mechanisms. Both these processes are directly related to wavelength of laser excitation. The shorter wavelength excitation provides improved laser–target coupling due to higher critical density ($n_c \alpha \lambda^{-2}$) and hence provides higher mass ablation rate. There are three

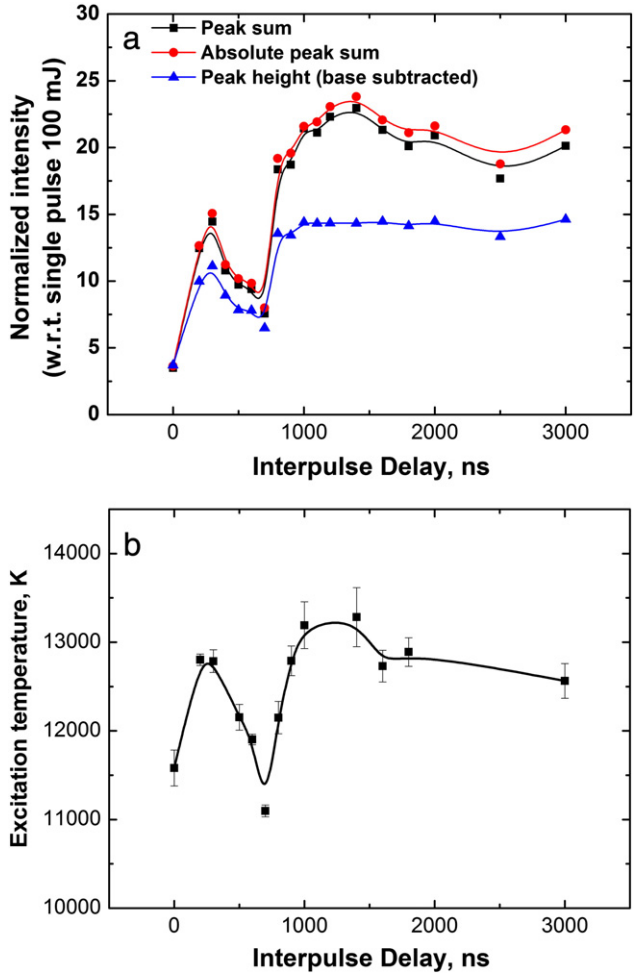

Fig. 4. (a) Signal enhancement observed for DPLIBS using YAG–YAG fundamental wavelength combination (E1 — 25 mJ, E2 — 75 mJ) with respect to single pulse LIBS (E — 100 mJ). Signal enhancement was calculated for three different signal-processing schemes (peak sum, absolute peak sum, peak height with base subtracted). (b) Excitation temperatures as a function of inter-pulse delay. Temperature was calculated using Boltzmann plots using Cu I atomic emission lines at 427.5 nm, 465.11 nm, 510.5 nm, 515.3 nm, and 521.8 nm. A gate delay of 1.4 μs after the second laser pulse was used for data acquisition.

main mechanisms of laser energy absorption by the plasma which include electron-ion inverse Bremsstrahlung, electron-neutral inverse Bremsstrahlung, and photoionization. The electron-ion inverse Bremsstrahlung is higher for longer wavelength excitation because of its λ^3 dependence while photoionization is more predominant at UV wavelengths. Considering transient nature of the plasma, it can concluded that both processes, viz. improved mass ablation and reheating, exist in collinear arrangement depending on inter-pulse delays. For very short delays, because of higher density of the pre-plume, the reheating will be more efficient while at larger inter-pulse delays, because of reduced density of the pre-plume, the laser target coupling will be higher which will lead to increased mass ablation. Signal enhancement could then be attributed to both the processes. For larger inter-pulse delays, most of the enhancement occurs due to increase in mass ablation. It has been showed in various shadowgraphy studies that after the laser strikes the target, shockwave is generated and most of the mass of the ambient gas is compressed in a thin layer at the shockwave front while inside the plume sudden pressure drop occurs presenting rarified ambient conditions [10,39,40]. As time progresses and shockwave front loses energy and pressure inside the plume core reaches its original ambient conditions. Reduced ambient gas density theory is also corroborated by observation of lack of ambient species (N, O) in core of the plume. It has been showed that second laser pulse generates new plasma on the target surface encompassed by the expanding plume front from the first laser pulse [8]. Due to rarified ambient conditions, the plasma expands rapidly and fills the entire plume area resulting in wider plume (approximately 3 times) as compared to single pulse.

Boltzmann plot was used to measure excitation temperature using Cu I lines, as showed in Fig. 4b. Similar trend in temperature is also observed as a function of inter-pulse delay. There is a dip in temperature and two maxima in peaks occur which correlates to the dual peak of signal enhancement. First peak occurs at ~250 ns while second maxima occur after ~1000 ns. It can be clearly seen that the signal enhancement follows excitation temperature trend for varying inter-pulse delays. The slower decay of temperature at higher inter-pulse delay is due to plasma confinement and larger extent of the hot spot region [8].

The signal enhancement dip noticed after 250 ns inter-pulse delay shows the reduced coupling between the pre-pulse plasma and reheating beam or reduction in laser–target interaction by the second

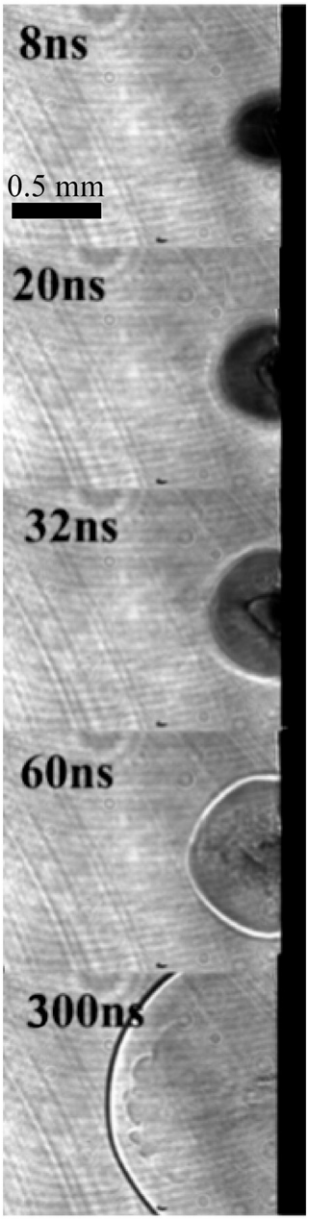

Fig. 5. Time evolution of shockwaves generated by the pre-plasma. Focused shadowgraphy is used to record the shadowgram. The laser wavelength and energy used in this experiment were 1064 nm and 25 mJ.

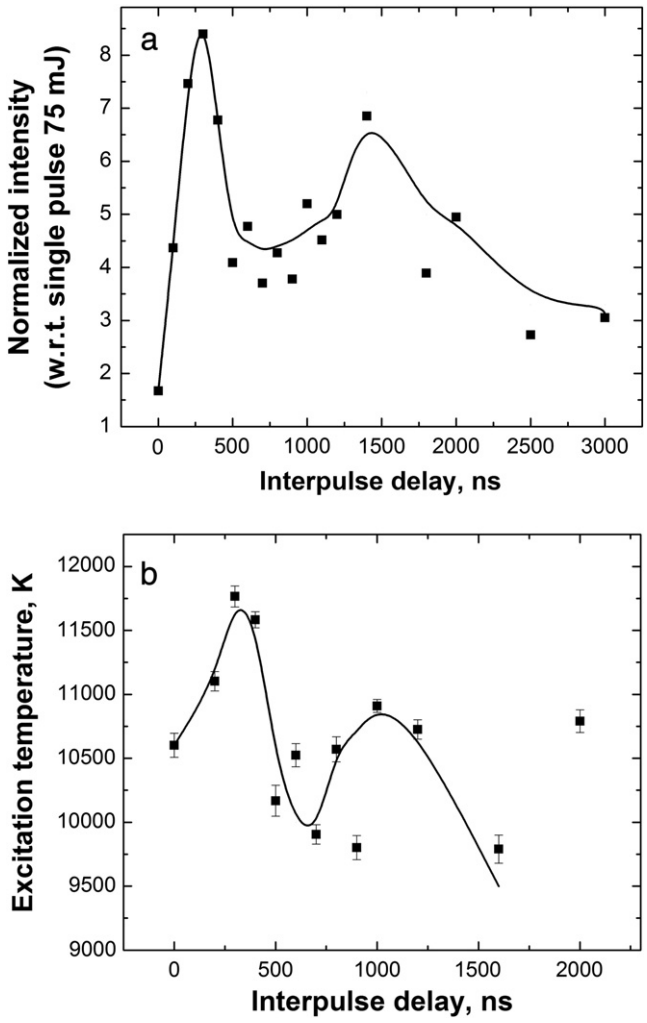

Fig. 6. a): Signal enhancement observed for DPLIBS using YAG–YAG fundamental wavelength combination (E1 — 25 mJ, E2 — 50 mJ) with respect to single pulse LIBS (E — 75 mJ). b) Excitation temperatures as a function of interpulse delay. Temperature was calculated using Boltzmann plots using Cu I atomic emission lines at 427.5 nm, 465.11 nm, 510.5 nm, 515.3 nm, and 521.8 nm. A gate delay of 1.4 μs after the second laser pulse was used for data acquisition.

beam. The interaction of the second laser pulse with the extremely rarified ambient conditions behind the shockwave front of the pre-plasma can reduce the emission intensity. According to previous studies [40–42], there exists an optimum rarefaction or buffer gas pressure range for which the emission intensity is maximum and this pressure at room temperature corresponds to ~110–750 Torr. The first laser pulse results in formation of shockwave front, which leads to decrease in buffer gas density behind the shockwave front. Decrease in ambient gas density close to the target surface leads to decrease in laser shielding by the pre-plasma thereby increasing the laser ablation and signal enhancement. The shockwave front detaches from the plume front after few hundreds of nanoseconds and travels further while the plume core gets stagnated at few mm from the plasma surface depending on the laser pulse energy [39]. At further inter-pulse delays (>500 ns), optimum rarified regions are obtained leading to signal enhancement mostly due to increase in mass ablation. Overall, signal enhancement can be attributed to a combination of increased laser ablation as well as reheating of the plume. The plasma formed by the second laser pulse expands at faster speed in rarified environment [8]. As can be seen, signal enhancement between 15 and 25 times can be achieved using YAG–YAG fundamental wavelength combination at optimum inter-pulse delay.

The signal enhancement dip observed with respect to inter-pulse delay is explained based on the condition of optimum rarified pressure in the pre-plasma for reheating. However, the shockwaves formed by the pre-plasma can also reduce the coupling between the reheating beam and pre-formed plasma or target for further ablation. The time evolution of the shockwaves generated by the pre-plasma is given in Fig. 5. Typically strong shockwaves are generated when laser ablation plasma is generated in the presence of 1 atm and the shock pressure can reach several 10s of atmosphere pressure and its pressure decreases rapidly with time [39]. The density jump created by the shock front can affect the coupling of the reheating laser with the pre-plume as well as the target, which can essentially lead to a dip in the signal enhancement. As time evolves, the shock pressure decreases rapidly which improves the coupling between the reheating pulse with pre-formed plasma and the target.

In the second set of experiments, ratio of laser pulse energies was changed. Prepulse laser energy was kept constant at 25 mJ while reheating laser pulse energy was changed to 50 mJ. Similar trend was observed for increase intensity for different inter-pulse delays with dual peaks and a dip in between as shown in Fig. 6. Although for this case, first peak was higher as compared to second peak. Since the laser pulse energy of *laser 2* is decreased, it is less efficient in reheating the laser plume as well as ablating the mass resulting in decrease in peak intensity. Signal enhancement is observed for delays up to 3 μs although the signal enhancement decreases with increase of inter-pulse delays. Temperature is also lower as compared to that shown in Fig. 4b.

3.3. Role of laser pre-pulse wavelength

Laser ablation wavelength has a significant influence on the laser produced plasma and plume morphology. Fig. 7 shows ICCD images for three different wavelengths on an Al sample using 25 mJ pulse energy. The image was taken at a delay of 30 ns after the first laser pulse. A definite difference in plume morphology, expansion, and aspect ratio of the plume can be observed. Laser produced plasma for 266 nm has a more hemi-spherical shape as compared to 1064 nm LPP. Figs. 5 and 7 imply that the second laser pulse will interact

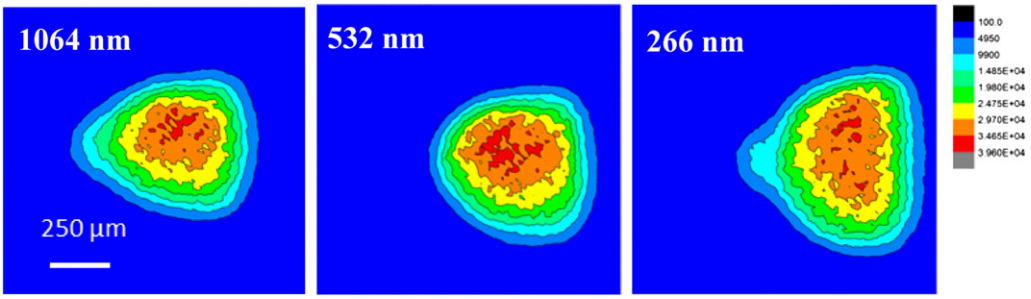

Fig. 7. Plume morphology showing plume expansion and emission hot spots for 1064 nm, 532 nm and 266 nm laser ablation wavelengths. Laser pulse energy of 25 mJ was used for ablating Al target. ICCD images were taken at a delay of 30 ns after the first laser pulse.

with different shockwave front as well as plume front depending on wavelength of the first laser pulse.

Fig. 8a–c shows the role of pre-pulse laser wavelength on signal enhancement. The 266 nm and 532 nm laser wavelengths were used as *laser 1* or prepulse laser followed by 1064 nm as *laser 2*. The signal is compared with single pulse LIBS using 266 nm or single pulse 532 nm. Optimum signal enhancement is observed at ~100 ns for 266 nm:1064 nm combination while for 532 nm:1064 nm, optimum interpulse delay is obtained ~500 ns after the second laser pulse, after which the enhancement decays. No dual peaks were observed for 266 nm:1064 nm combination while for 532 nm:1064 nm a slight dip in enhancement was observed around ~200 ns inter-pulse delay. UV laser pulse is efficient in coupling to the target because of reduced shielding effects resulting in increased mass ablation as compared to NIR pulses. Shockwave front as well as plume morphology is different for NIR, visible and UV pulses as showed in ICCD images above. The 1064 nm laser pulse then interacts with rarified ambient conditions, which further ablates the target as well as re-heats or excites the plasma plume from *laser1* (266 nm or 532 nm). Signal enhancement occurs even for extremely long inter-pulse delays, especially for 266 nm as pre-pulse compared to pre-pulses generated by 532 nm and 1064 nm and this could be due to increased ablated mass by 266 nm laser pulse. As compared to 1064 nm and 532 nm, 266 nm results in better absolute signal intensity (~5× and ~3× respectively) which again can be attributed to increase in mass ablation, higher temperature and electron density due to multi-photon ionization-driven nature of LIBS plasma generated by UV laser pulse followed by re-heating and/or further ablation by NIR pulse.

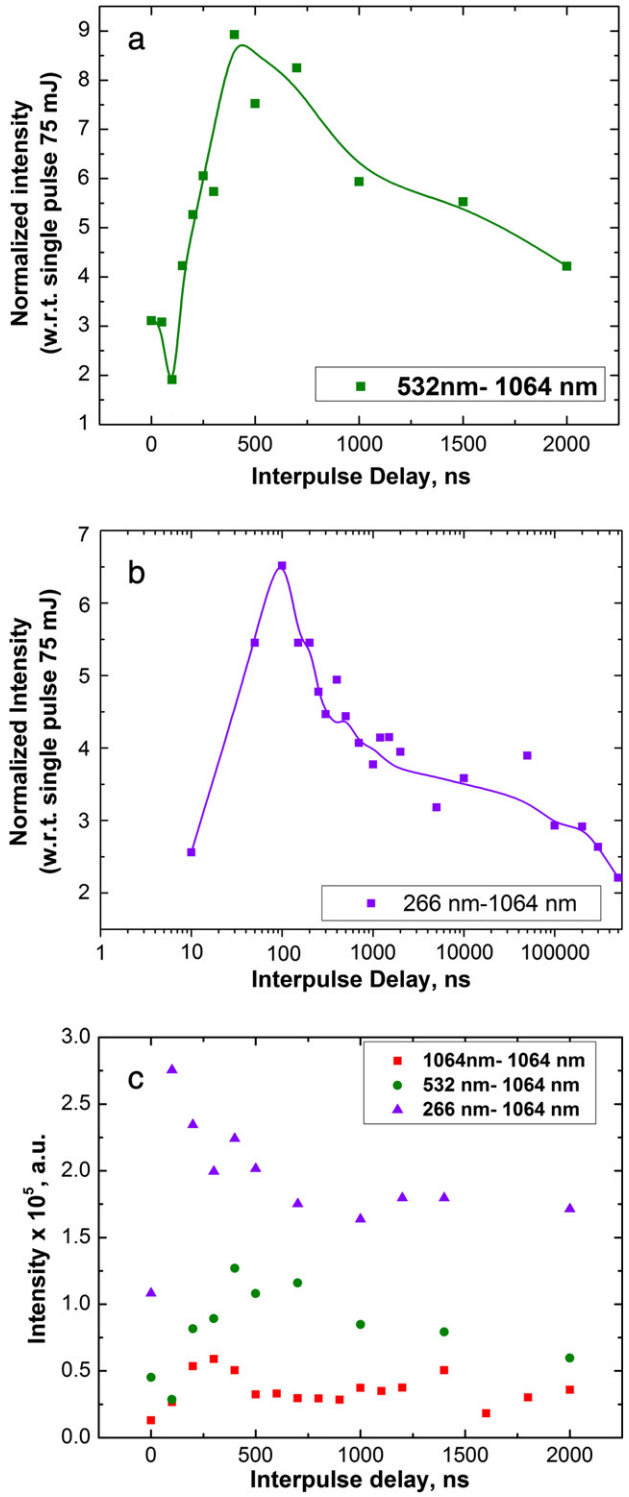

Fig. 8. Signal enhancement (Cu I 521.8 nm) observed for DPLIBS using YAG–YAG a) 532 nm:1064 nm and b) 266 nm:1064 nm wavelength combination (E1 — 25 mJ, E2 — 50 mJ) with respect to single pulse LIBS (E — 75 mJ). c) Absolute integrated signal intensity for three different pre-ablation wavelengths. A gate delay of 1.4 μs after the second laser pulse was used for data acquisition.

3.4. Persistence of plasma species

Many studies have showed that the emission lifetime is longer in DPLIBS. As recommended in a recent LIBS review [43], the term 'persistence' is being used to describe the emission decay or emission lifetime of Cu and Zn neutral species. Fig. 9 shows the comparison of 'persistence' of neutral species (Cu I, 521.8 nm) in DPLIBS and single pulse LIBS. Time of flight emission spectroscopy was used to measure the persistence of Cu I species, which was observed to be larger (~2×x) in the case of DPLIBS. Similar enhancement in persistence was observed for Zn I species as well, although the enhancement in persistence was more pronounced for Cu I line at 521.8 nm. The persistence is further enhanced for UV–NIR combination of DPLIBS that explains longer lasting DPLIBS signal.

4. Electron density measurements

Stark broadening method was used for estimation of electron density using Zn I line at 481 nm. Electron density is directly related to full width half maximum (FWHM) of stark broadened emission line which consists of contributions from both ionic as well as electronic terms. For nonhydrogenic species, contribution from ionic term can be neglected and simplified equation can be written as follows: [44]

$$\Delta\lambda_{1/2} = 2w\left(N_e/10^{16}\right)\text{Å} \quad (1)$$

where $\Delta\lambda_{1/2}$ is FWHM of the emission line in Å unit and w is the electron impact parameter which is a function of plasma temperature and can be found using reference literature [45]. Line width was corrected for instrumental broadening (0.025 nm) while pressure and Doppler broadening were ignored as their effect is assumed to be negligible. A Lorentzian fit was provided to the raw spectra to measure the full width half maximum (FWHM) of the Zn I line. Electron density for double pulse LIBS is found to be higher as compared to single pulse LIBS (Fig. 10a–b). Most of the DPLIBS studies have showed a decrease in electron density at early signal acquisition times followed by a slower decay as compared to single pulse LIBS [36]. In most of these studies the signal was integrated spatially. In this study, the emission was observed at 1 mm from the target; additionally the electron density reported here is at a delay of 1400 ns after the second laser pulse. At this gate delay, it is possible that the electron density for double

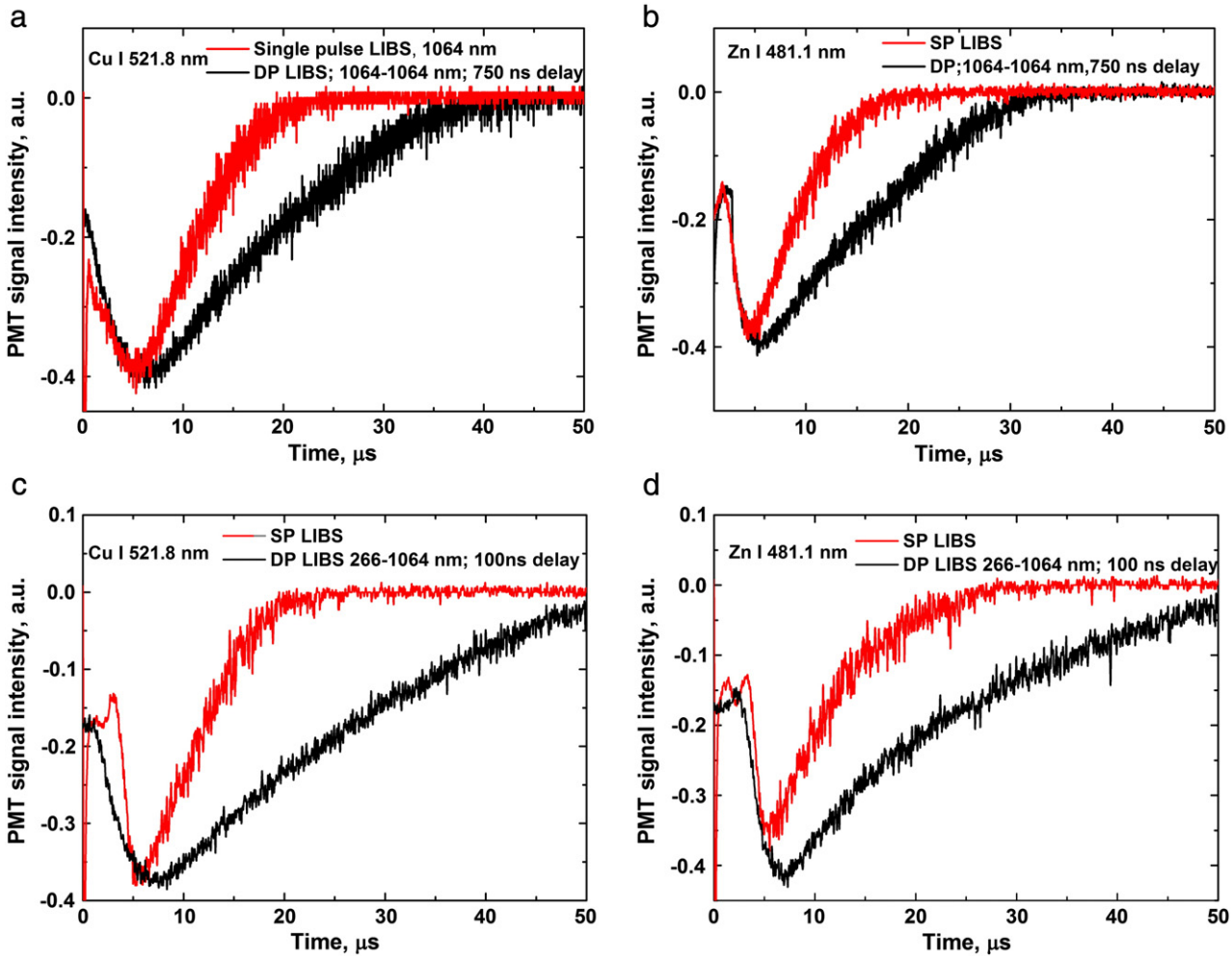

Fig. 9. Persistence of neutral species. Optical time-of-flight profile of Cu I and Zn I recorded at 1 mm from target for DPLIBS a) Cu I 1064 nm:1064 nm; 25:75 mJ and single pulse LIBS (1064 nm; 100 mJ) b) Zn I 1064 nm:1064 nm; 25:75 mJ and single pulse LIBS (1064 nm; 100 mJ) c) Cu I 266 nm:1064 nm; 25:50 mJ and single pulse LIBS (266 nm; 75 mJ) d) Zn I 266 nm:1064 nm; 25:50 mJ and single pulse LIBS (266 nm; 75 mJ).

pulse to be higher as compared to single pulse due to slower decay of the electron density for DPLIBS case as observed by Colao et al. [36]. Higher electron density can also be due to higher mass ablation due to better laser–target coupling. This is supported by higher densities observed for 266–1064 nm combination compared to 1064–1064 nm. Similar electron density trend is observed as a function of inter-pulse delays.

5. Conclusions

DPLIBS has been one of many approaches for improving the analytical performance of LIBS technique. Signal enhancement can be obtained by employing any of the DPLIBS configurations, although the mechanisms and processes involved in signal enhancement differ and are not clearly understood. Inter-pulse delay, laser pulse energy and laser wavelength are important parameters which influence signal enhancement. Depending on the inter-pulse delay and pre-pulse laser wavelength, different mechanisms are involved in signal enhancement. Signal enhancement was observed even at zero inter-pulse delay. For NIR:NIR combination, dual peaks in signal enhancement were observed as a function of inter-pulse delay. A decrease in signal enhancement was observed after 250 ns, which correlated with the decrease in plasma excitation temperature as measured using Boltzmann method using Cu I lines. The decrease could be due to the interaction of the second laser pulse with extremely rarified plume resulting in the decrease of the temperature, even though mass ablation might not be affected. Following this inter-pulse regime, second peak occurs. In this regime, the plasma from the first laser pulse is practically transparent to the second laser pulse; thereby the enhancement is mostly due to increase in mass ablation due to efficient ablation in rarified ambient environment. The plasma formed by the second laser pulse expands rapidly in the rarified ambient conditions leading to expansion of the plasma volume. The signal enhancement then continues for large interpulse delays.

A comparison between three pre-pulse wavelengths (266 nm, 532 nm and 1064 nm) showed distinct signal enhancement profiles with respect to inter-pulse delay. 266 nm:1064 nm combination resulted in maximum absolute signal intensity as compared to NIR:NIR and VIS:NIR combinations. Persistence of neutral species, both Cu and Zn, was increased by approximately two times for double pulse. UV:NIR combination resulted in larger increase in persistence of the species. Increase in plasma temperature as well as electron density was observed for double pulse case. Electron density was slightly higher for UV:NIR combination.

Acknowledgments

This work is partially supported by the US DOE National Nuclear Security Administration under award number DE-NA0001174.

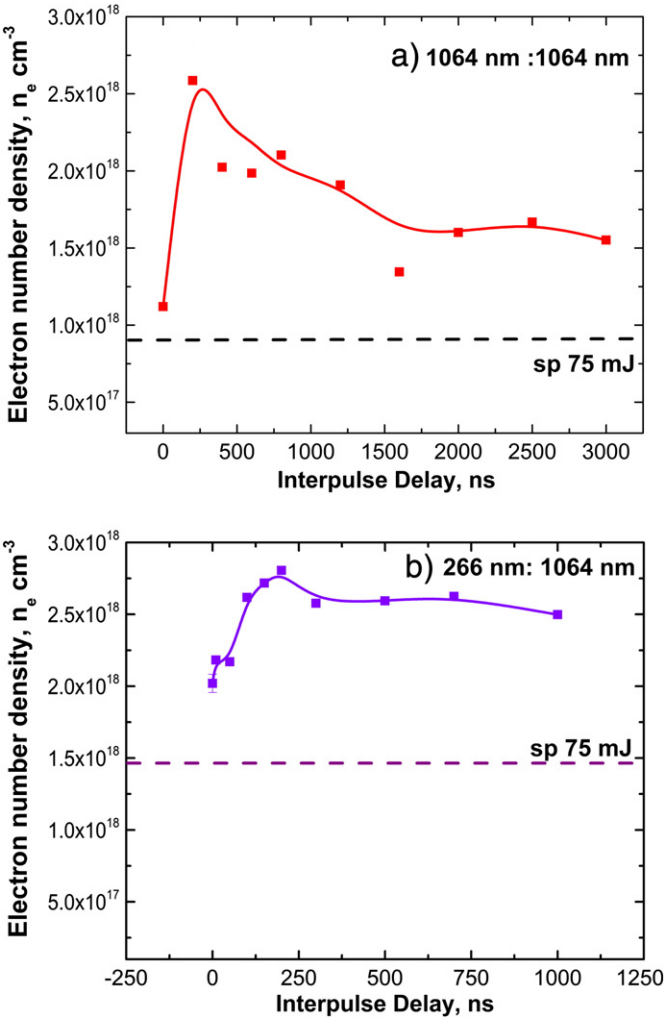

Fig. 10. Electron density as a function of interpulse delays for a) 1064 nm:1064 nm and b) 266 nm:1064 nm combinations. Stark broadening of Zn I line at 481 nm was used for estimation of electron density. A gate delay of 1.4 μs after the second laser pulse was used for data acquisition. Electron density estimated for single pulse LIBS is shown as dashed line.

References

[1] J.D. Winefordner, I.B. Gornushkin, T. Correll, E. Gibb, B.W. Smith, N. Omenetto, Comparing several atomic spectrometric methods to the super stars: special emphasis on laser induced breakdown spectrometry, LIBS, a future super star, J. Anal. At. Spectrom. 19 (2004) 1061–1083.

[2] M. Sabsabi, Laser-Induced Breakdown Spectroscopy, Elsevier, 2007.

[3] A.W. Miziolek, V. Palleschi, I. Schechter, LIBS Fundamentals and Applications, Cambridge Press, 2006.

[4] A. Santagata, R. Teghil, G. Albano, D. Spera, P. Villani, A. De Bonis, G.P. Parisi, A. Galasso, fs/ns dual-pulse LIBS analytic survey for copper-based alloys, Appl. Surf. Sci. 254 (2007) 863–867.

[5] Y.B. Zhao, S. Singha, Y.M. Liu, R.J. Gordon, Polarization-resolved laser-induced breakdown spectroscopy, Opt. Lett. 34 (2009) 494–496.

[6] V.I. Babushok, F.C. DeLucia, J.L. Gottfried, C.A. Munson, A.W. Miziolek, Double pulse laser ablation and plasma: laser induced breakdown spectroscopy signal enhancement, Spectrochim. Acta, Part B 61 (2006) 999–1014.

[7] A. Bogaerts, Z. Chen, D. Autrique, Double pulse laser ablation and laser induced breakdown spectroscopy: a modeling investigation, Spectrochim. Acta, Part B 63 (2008) 746–754.

[8] M. Corsi, G. Cristoforetti, M. Giuffrida, M. Hidalgo, S. Legnaioli, V. Palleschi, A. Salvetti, E. Tognoni, C. Vallebona, Three-dimensional analysis of laser induced plasmas in single and double pulse configuration, Spectrochim. Acta, Part B 59 (2004) 723–735.

[9] F.C. De Lucia, J.L. Gottfried, C.A. Munson, A.W. Miziolek, Double pulse laser-induced breakdown spectroscopy of explosives: initial study towards improved discrimination, Spectrochim. Acta, Part B 62 (2007) 1399–1404.

[10] R. Noll, R. Sattmann, V. Sturm, S. Winkelmann, Space and time resolved dynamics of plasmas generated by double pulses interacting with metallic targets, Spectrochim. Acta, Part B 19 (2004) 419–428.

[11] V.N. Rai, F.Y. Yueh, J.P. Singh, Theoretical model for double pulse laser-induced breakdown spectroscopy, Appl. Optics 47 (2008) G30–G37.

[12] G. Cristoforetti, S. Legnaioli, V. Palleschi, A. Salvetti, E. Tognoni, Influence of ambient gas pressure on LIBS technique in the parallel DP configuration, Spectrochim. Acta, Part B 59 (2004) 1907–1917.

[13] A. De Giacomo, M. Dell'Aglio, D. Bruno, R. Gaudiuso, O. De Pascale, Experimental and theoretical comparison of single-pulse and double-pulse laser induced breakdown spectroscopy on metallic samples, Spectrochim. Acta, Part B 63 (2008) 805–816.

[14] J.L. Gottfried, F.C. De Lucia, C.A. Munson, A.W. Miziolek, Double-pulse standoff laser-induced breakdown spectroscopy for versatile hazardous materials detection, Spectrochim. Acta, Part B 62 (2007) 1405–1411.

[15] J. Goujon, A. Giakoumaki, V. Pinon, O. Musset, D. Anglos, E. Georgiou, J.P. Boquillon, A compact and portable laser-induced breakdown spectroscopy instrument for single and double pulse applications, Spectrochim. Acta, Part B 63 (2008) 1091–1096.

[16] S. Nakamura, Y. Ito, K. Sone, H. Hiraga, K. Kaneko, Determination of an iron suspension in water by laser-induced breakdown spectroscopy with two sequential laser pulses, Anal. Chem. 68 (1996) 2981–2986.

[17] A.E. Pichahchy, D.A. Cremers, M.J. Ferris, Elemental analysis of metals under water using laser-induced breakdown spectroscopy, Spectrochim. Acta, Part B 52 (1997) 25–39.

[18] L. St-Onge, V. Detalle, M. Sabsabi, Enhanced LIBS using combination of fourth harmonic and fundamental YAG laser pulses, Spectrocmimica Acta B 57 (2002) 121–135.

[19] L. St-Onge, M. Sabsabi, P. Cielo, Analysis of solids using laser-induced plasma spectroscopy in double-pulse mode, Spectrochim. Acta A Mol. Biomol. Spectrosc. 53 (1998) 407–415.

[20] A.A. Andreev, J. Limpouch, A.B. Iskakov, H. Nakano, Enhancement of x-ray line emission from plasmas produced by short high-intensity laser double pulses, Phys. Rev. E 65 (2002), 026403.

[21] M.C. Chou, P.H. Lin, H.E. Tsai, D.L. Chen, C.H. Lee, J.Y. Lin, J. Wang, S.Y. Chen, Characterization and control of plasma density distribution for the development of solid-target x-ray lasers, Phys. Rev. E 72 (2005), 026407.

[22] J.R. Freeman, S.S. Harilal, A. Hassanein, B. Rice, Effect of prepulse laser wavelength on EUV emission from CO2 reheated laser-produced Sn plasma, Appl. Phys. A 110 (2013) 853–856.

[23] J.R. Freeman, S.S. Harilal, A. Hassanein, Extreme ultraviolet emission enhancements from a prepulsed Sn laser-produced plasma, J. Appl. Phys. 110 (2011) 083303.

[24] G. Cristoforetti, S. Legnaioli, V. Palleschi, A. Salvetti, E. Tognoni, Characterization of a collinear double pulse laser-induced plasma at several ambient gas pressures by spectrally- and time-resolved imaging, Appl. Phys. B Lasers Opt. 80 (2005) 559–568.

[25] P. Dunne, G. O'Sullivan, D. O'Reilly, Prepulse-enhanced narrow bandwidth soft x-ray emission from a low debris, subnanosecond, laser plasma source, Appl. Phys. Lett. 76 (2000) 34–36.

[26] D.N. Stratis, K.L. Eland, S.M. Angel, Effect of pulse delay time on a pre-ablation dual-pulse LIBS plasma, Appl. Spectrosc. 55 (2001) 1297–1303.

[27] A. Kuwako, Y. Uchida, K. Maeda, Supersensitive detection of sodium in water with use of dual-pulse laser-induced breakdown spectroscopy, Appl. Opt. 42 (2003) 6052.

[28] D.K. Killinger, S.D. Allen, R.D. Waterbury, C. Stefano, E.L. Dottery, Enhancement of Nd:YAG LIBS emission of a remote target using a simultaneous CO_2 laser pulse, Opt. Express 15 (2007) 12905–12915.

[29] R.W. Coons, S.M. Hassan, S.S. Harilal, A. Hassanein, The importance of longer wavelength reheating in dual-pulse laser-induced breakdown spectroscopy, Appl. Phys. B Lasers Opt. 107 (2012) 873–880.

[30] J. Uebbing, J. Brust, W. Sdorra, F. Leis, K. Niemax, Reheating of a laser-produced plasma by a second pulse laser, Appl. Spectrosc. 45 (1991) 1419.

[31] D.N. Stratis, K.L. Eland, S.M. Angel, Dual-pulse LIBS using a pre-ablation spark for enhanced ablation and emission, Appl. Spectrosc. 54 (2000) 1270–1274.

[32] V. Hohreiter, D.W. Hahn, Dual-pulse laser induced breakdown spectroscopy: time-resolved transmission and spectral measurements, Spectrochim. Acta B At. Spectrosc. 60 (2005) 968–974.

[33] R.D. Waterbury, A. Pal, D.K. Killinger, J. Rose, E.L. Dottery, G. Ontai, Standoff LIBS measurements of energetic materials using a 266 nm excitation laser — art. no. 695409, Proc. SPIE 6954 (2008) 695409.

[34] X. Mao, X. Zeng, S. Wen, R.E. Russo, Time resolved plasma properties for DP LIBS of Si, Spectrochim. Acta, Part B 60 (2005) 960–967.

[35] D.N. Stratis, K.L. Eland, S.M. Angel, Enhancement of aluminum, titanium, and iron in glass using pre-ablation spark dual-pulse LIBS, Appl. Spectrosc. 54 (2000) 1719–1726.

[36] F. Colao, V. Lazic, R. Fantoni, S. Pershin, A comparison between Single pulse and DP LIBS of Al samples, Spectrochim. Acta, Part B 57 (2002) 1167.

[37] C. Gautier, P. Fichet, D. Menut, J.L. Lacour, D. L'Hermite, J. Dubessy, Study of the double-pulse setup with an orthogonal beam geometry for laser-induced breakdown spectroscopy, Spectrochim. Acta, Part B 59 (2004) 975–986.

[38] C. Gautier, P. Fichet, D. Menut, J.L. Lacour, D. L'Hermite, J. Dubessy, Main parameters influencing the double-pulse laser-induced breakdown spectroscopy in the collinear beam geometry, Spectrochim. Acta, Part B 60 (2005) 792–804.

[39] S.S. Harilal, G.V. Miloshevsky, P.K. Diwakar, N.L. LaHaye, A. Hassanein, Experimental and computational details of laser ablation plumes at atmospheric pressure, Physics of Plasmas 19 (2012) 083504.

[40] G. Cristoforetti, S. Legnaioli, L. Pardini, V. Palleschi, A. Salvetti, E. Tognoni, Spectroscopic and shadowgraphic analysis of laser induced plasmas in the orthogonal double pulse pre-ablation configuration, Spectrochim. Acta, Part B 61 (2006) 340–350.
[41] P.A. Benedetti, G. Cristoforetti, S. Legnaioli, V. Palleschi, L. Pardini, A. Salvetti, E. Tognoni, Effect of laser pulse energies in laser induced breakdown spectroscopy in double-pulse configuration, Spectrochim. Acta, Part B 60 (2005) 1392–1401.
[42] W. Sdorra, K. Niemax, Basic investigations for laser microanalysis. 3. Application of different buffer gases for laser-produced sample plumes, Mikrochim. Acta 107 (1992) 319–327.
[43] D.W. Hahn, N. Omenetto, Laser-induced breakdown spectroscopy (LIBS), part II: review of instrumental and methodological approaches to material analysis and applications to different fields, Appl. Spectrosc. 66 (2012) 347–419.
[44] H.R. Griem, Plasma Spectroscopy, McGraw-Hill, New York, 1964.
[45] M.S. Dimitrijevic, S. Sahal-Brechot, Stark broadening of neutral zinc spectral lines, Astronomy & Astrophysics Supplement Series 140 (1999) 193–196.